

CHAPTER 61

NUMERICAL SIMULATION OF TSUNAMIS ORIGINATING IN THE PERU-CHILE TRENCH

BY

A. W. Garcia¹ and H. L. Butler²

I. Introduction

1. The U. S. Army Corps of Engineers has as an objective of its research and development program the determination of better harbor design criteria for tsunami protection. A previous report (Houston, et. al., 1975b) addressed the subject of tsunami vulnerability of the Pacific Coast of the continental United States to tsunamis originating in the Aleutian Trench. That report determined the variation in tsunami amplitude as a function of coastal distance due to a standard uplift source at different locations in the Aleutian Trench. The present report is a continuation of that study and addresses the subject of tsunami vulnerability along the same stretch of coast to tsunamis originating in the Peru-Chile Trench. In addition, modifications to the numerical code used in the previous report allowed the simulation of the Chile tsunami of May 22, 1960.

II. Historical Narrative

2. There have been four well documented major tsunamis to strike the Pacific Coast of the United States in recent times; the Great Aleutian tsunami of 1946, the Alaska tsunami of 1957, the Chile tsunami of 1960 and the Alaska tsunami of 1964. The 1964 Alaska tsunami claimed 107 lives in Alaska, 4 in Oregon and 11 in Crescent City, California. In addition to 330 lives in Chile, the 1960 Chile tsunami claimed 61 in Hawaii and 199 in Japan. Table 1 (Symons, et al., 1960) shows a comparison of maximum wave heights for the tsunamis of 1946, 1952, 1957, and 1960. The comparative intensity of the 1960 tsunami is evident. Indeed, the generating earthquake was of magnitude 8.6, one of the largest ever recorded.

3. The association of large submarine earthquakes with island arcs and deep submarine trenches is well documented (Kelleher, et. al., 1974; Kelleher, 1972; Sykes, 1971). The Japan-Kurile-Kamchatka, the Aleutian and the Peru-Chile Trench regions have long recorded histories of tsunamigenic activity. Of these, however, only tsunamis originating in the Aleutian and Peru-Chile Trenches have a history of causing significant runup along the Pacific Coast of the United States. Because tsunamis originating in the Aleutian Trench is the subject of a previous report, (Houston, et. al., 1975b) it will not be recounted here.

¹Research Oceanographer, USAE Waterways Experiment Station, Vicksburg, MS.

²Research Physicist, USAE Waterways Experiment Station, Vicksburg, MS.

Table 1
Maximum Recorded Rise or Fall

(This table lists only places at which gages were operating during all four tsunamis)

Station	1946	1952	1957	1960
	Feet	Feet	Feet	Feet
Honolulu, Hawaii	4.1	4.4	3.2+*	5.5+*
Sitka, Alaska	2.6	1.5	2.6	3.0
Neah Bay, Wash.	1.2	1.5	1.0	2.4
Crescent City, Calif.	5.9	6.8	4.3	10.9
San Francisco, Calif.	1.7	3.5	1.7	2.9
Port Hueneme, Calif.	5.5	4.7	3.5	8.8
Los Angeles (Berth 60), Calif.	2.5	2.0	2.1	5.0
La Jolla, Calif.	1.4	0.8	2.0	3.3
San Diego, Calif.	1.2	2.3	1.5	4.6

*Measured rise or fall. No extrapolation made for height beyond gage limit.

4. There is some evidence, however, to indicate that Richter scale magnitudes tend to underestimate the source parameters (fault length, width and uplift) and thus the tsunamigenic potential of very large earthquakes. Cumulative frequency vs. surface wave magnitude (M_s) plots show a linear trend for earthquakes with M_s values less than about 7.0 but for higher values of M_s the locus becomes increasingly steep tending toward vertical at M_s approximately equal 8.6. Therefore, it has been commonly assumed earthquakes with M_s greater than about 8.6 do not occur which may indeed be true. This, however, does not necessarily imply there is an upper limit on earthquake source parameters. Conventional analyses of earthquake energy spectra to determine M_s are frequency dependent. Chinnery and North (1975) hypothesize that because very large earthquakes produce spectra that have significant proportions of energy at frequencies below the band where M_s is normally measured and have dislocations which propagate for times significantly greater than 20 seconds that an upper limit to M_s will be observed no matter how large the true earthquake size.

III: Peru-Chile Trench As A Tsunamigenic Region

5. In terms of plate tectonics, the shallow seismic zone of western South America is a continuous boundary along which one plate (the Nazca plate) underthrusts the adjacent plate (the Americas plate). Kelleher (1974) cites numerous studies that indicate this plate motion is accomplished by large magnitude earthquakes, consequently any segment of the boundary that has not ruptured for many decades should be considered a zone of high risk. Moreover, Kelleher (1972) has observed that about once each century the entire fault segment near the Central Valley province

of central and southern Chile (approx. 32° -- 46° S) has fractured in a general north-south direction by a progression of large earthquakes and hypothesizes that a new series of quakes might start about the end of this century near Valparaiso (33° S) and progress southward.

6. Hayes (1966) states that crustal thinning beneath the trench is evidence the major tectonic forces involved are not laterally compressive and the absence of these compressive forces can be produced by a combination of faulting and flexure in the transition region of an ocean-continent margin. He also observes that almost all quake epicenters in the area lie shoreward of the axis of the trench.

7. Plafker and Savage (1970) report that records kept by the Japanese suggest that the subsea tectonic displacement of the 1960 Chile earthquake is probably greater than those associated with any of the earlier earthquakes during a period of nearly 500 years. Indeed, vertical movements of a larger regional scale appear to be characteristic of that portion of the trench extending from Columbia to southern Chile.

IV. Tsunami Source Characteristics

8. Figure 1 shows the contours of elevation of the initial sea surface deformation used as input to the simulation of the Chile tsunami of May 22, 1960. The shape of the deformation is inferred from the works of Plafker and Savage (1970) and Hwang, et. al., (1970). Plafker and Savage show the maximum upward vertical displacement of their preferred interpretation of the fault model to be about 10 m although the maximum observed upward vertical displacement was about 6 m. To avoid distorting the large scale features, the available data were smoothed, that is the maximum vertical uplift of 24 ft was chosen to compromise between the maximum predicted uplift of 10 m and maximum observed uplift of 6 m. Because the data indicate there was little downthrow (less than 2 m) associated with the tectonic deformation this feature was neglected in the model. The length of the deformation was determined from the spatial distribution of the epicenters of the initial quake and aftershocks as shown in Plafker and Savage (1970) and both its meridional and latitudinal extent are consistent with the area of the rupture zone as shown in Figure 2 (from Kelleher et. al., 1974).

9. There is little question that the deformation used for the simulation of the 1960 Chile tsunami is not known with the confidence of that used to simulate the Alaska tsunami of March 28, 1964. Nonetheless, there are enough data available to credibly reconstruct the bottom deformation which generated the tsunami.

10. Figure 3 shows the idealized axis of the Peru-Chile Trench as divided into 12 segments. A hypothetical sea surface deformation which generates a tsunami of approximately four intensity is centered in and aligned with segments one, eight and twelve. In order to facilitate comparison with results of a previous study (Houston, et. al., 1975b), the present hypothetical uplift is identical to that of the previous study.

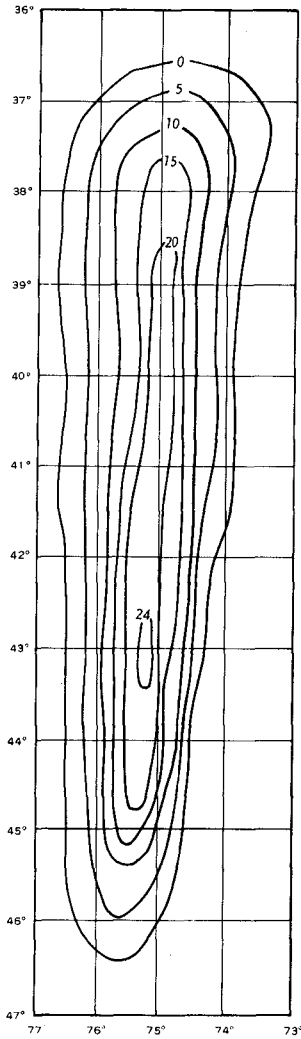


Figure 1. Contours of elevation of uplift used to simulate 1960 Chile earthquake.

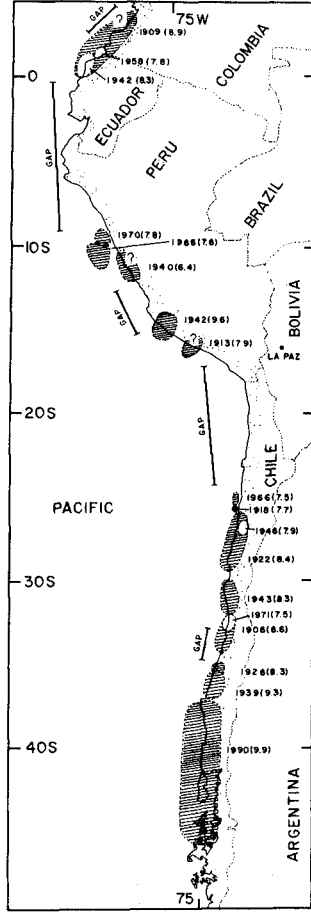
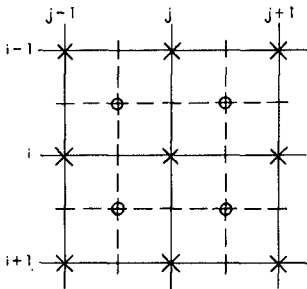


Figure 2. Rupture zones for large shallow earthquakes of this century and existing seismic gaps (after Kelleher, et. al., 1972).

SOUTH
PACIFIC OCEAN



LEGEND

- x - WATER ELEVATION, η
- o - WATER DEPTH, d
- - U VELOCITY IN DIRECTION, θ
- | - V VELOCITY IN DIRECTION, ϕ

Figure 4. Graphic representation of the finite difference grid.

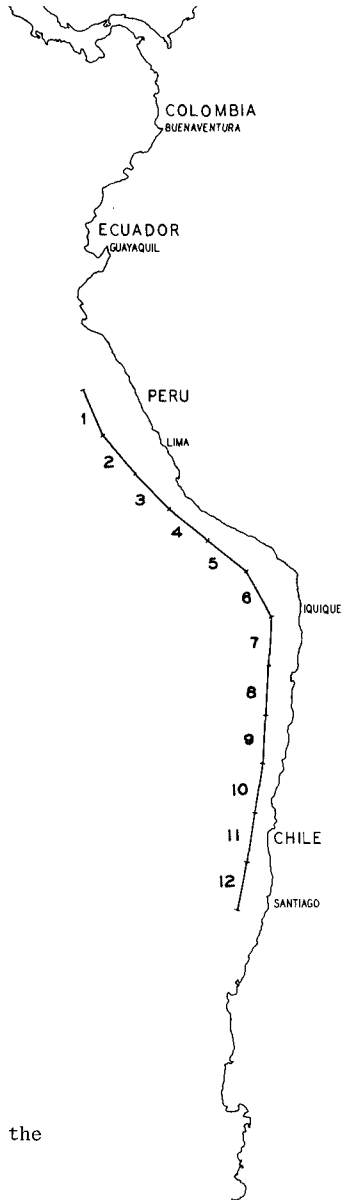


Figure 3. Idealized axis of Peru-Chile Trench showing 12 segments.

V. Computational Model

11. The numerical code used to simulate the 1960 Chile tsunami and the idealized hypothetical disturbances is based upon the linearized longwave equations obtained by vertically integrating the Navier-Stokes equations and equation of continuity. The equations used in the code are formulated in a spherical system as follow:

$$\frac{\partial U}{\partial t} = - \frac{g}{R_e} \frac{\partial \eta}{\partial \theta} \quad (1)$$

$$\frac{\partial V}{\partial t} = - \frac{g}{R_e \sin \phi} \frac{\partial \eta}{\partial \phi} \quad (2)$$

$$\frac{\partial \eta}{\partial t} = - \frac{1}{R_e \sin \phi} \left\{ \frac{\partial}{\partial \theta} (\eta+d) U \sin \theta + \frac{\partial}{\partial \phi} (\eta+d) V \right\} \quad (3)$$

where

U = depth-averaged wave velocity component in the θ direction

V = depth-averaged wave velocity component in the ϕ direction

g = acceleration due to gravity

R_e = radius of earth

η = wave elevation from reference water level

θ = latitude measured positive from north pole

ϕ = longitude measured positive eastward from Greenwich

d = local water depth

The validity of using linearized equations and the conditions under which they hold are discussed in Houston, et. al., (1975b).

12. In order to facilitate simulation of the tsunami of May 22, 1960, modifications were made to the code used for previous reports (Houston and Garcia, 1974; Garcia and Houston, 1975, Houston et. al., 1975b) to permit larger grids and faster execution. In the above mentioned reports the finite difference forms of Equations 1, 2, and 3 were solved by an alternating direction multistep technique whereby during the first half-time step, η and U were computed implicitly along lines of constant longitude and V explicitly along lines of constant latitude; in the second half-time step η and V are computed implicitly along line of constant latitude and U explicitly along lines of constant longitude. In the present report, Equations 4-6 are the finite difference forms of Equations 1-3.

$$U_{i,j}^{n+1/2} = U_{i,j}^{n-1/2} - \frac{g \Delta t}{R_e \Delta \theta} (\eta_{i+1,j} - \eta_{i,j})^n \quad (4)$$

$$V_{i,j}^{n+1/2} = V_{i,j}^{n-1/2} - \frac{g \Delta t}{R_e \Delta \phi \sin \theta} (\eta_{i,j+1} - \eta_{i,j})^n \quad (5)$$

$$\eta_{i,j}^{n+1} = \eta_{i,j}^n - \frac{1}{R_e \sin \theta} \left\{ \frac{\Delta t}{\Delta \theta} \left[(U d \sin \theta)_{i,j} - (U d \sin \theta)_{i-1,j} \right]^{n+1/2} + \frac{\Delta t}{\Delta \phi} \left[(V d)_{i,j} - (V d)_{i,j-1} \right]^{n+1/2} \right\} \quad (6)$$

(where it is assumed $n \ll d$)

Figure 4 shows the grid scheme used. The depth, d , is considered the averaged depth over the grid square j to $j+1$, i to $i+1$. Equations 4 and 5 are solved explicitly at the same halftime step along lines of constant longitude and latitude respectively. Equation 6 is then solved for η onehalf time step later. The boundary conditions, reflective at land boundaries and transmissive at the open ocean grid boundaries, are treated in the same manner as in the previous report (Houston, et. al., 1975b).

13. The explicit code was verified by comparing the results of hindcasting the Alaska tsunami of March 28, 1964 with results of hindcasting the same tsunami using the earlier implicit-explicit code. There was almost exact agreement of the results.

14. To further reduce the computational time required and to allow a greater area to be covered, a one-third by one-third degree grid was used instead of the onethird by one-fifth degree grid used in the previous report (Houston, et. al., 1975b). The validity of using the coarser grid to propagate tsunamis over the open ocean has been demonstrated by Houston, et. al., (1975a). Use of the latest bathymetric information for the Pacific Coast of the United States allows significant improvement in the detailing of the coastline and continental shelf area.

15. Depths for the open ocean portion of the numerical grid were interpolated from data of ocean depths averaged over areas of one-degree squares of latitude and longitude (Smith, et. al., 1966) available from the National Oceanographic Data Center. Normally, the numerical code interpolates depth data from one point per square degree to nine points per square degree. However, for the continental shelf area, the interpolation process was not used; instead data taken directly from bathymetric charts in a form compatible with the numerical code were inserted.

16. By the modifications made to the finite difference form of the equations used in the numerical code and the use of coarser depth grid, the computational time for similar problems is reduced by a factor of approximately three relative to the previous code.

VI. Procedure

17. To locate the hypothetical uplifts, the Peru-Chile Trench was divided in twelve equal segments as shown in Figure 3. An uplift of the same configuration used in the previous report (Houston, et. al., 1975b) was centered in segments 1, 8 and 12. Segment 1, although closest to the Pacific Coast of the continental United States, is least favorably oriented for producing large waves which propagate in that direction. Segment 8, although more favorably oriented for production of large waves, would be the segment most influenced by the "shadowing" effect of the reach of coast immediately northward of the perimeter of the uplift area. In principle, an uplift centered in segment 7 would experience more shadowing effect, but the uplift placed there would have had a significant proportion on land and therefore produce a smaller tsunami. The orientation of segment 12 is very similar to that of segment 8, that is, more favorably oriented than segment 1 for production of large waves in the direction of the United States, but without the "shadowing" effect experienced by segment 8. One therefore would expect the overall amplitudes of the tsunamis arriving at the Pacific Coast of the United States to be least for those produced by the uplift centered in segment 8 (excluding segment 7) with tsunamis originating in the remaining eight segments producing values between those of segments 1 and 12.

18. To compare the amplitude of the leading wave of the tsunami generated by the three hypothetical ground motions as a function of distance along the Pacific coast of the United States, the amplitudes were normalized to a depth of 600 ft. This is done by analytically solving a one-dimensional standing wave equation (Lamb, 1932). This is done in detail in (Houston et. al., 1975b) but will be recounted briefly here.

19. Combining the one-dimensional long-wave equation of motion and the continuity equation (in rectangular coordinates) yields the wave equation

$$\frac{\partial^2 \eta(x)}{\partial t^2} = g \frac{\partial}{\partial x} d \frac{\partial \eta(x)}{\partial x} \quad (7)$$

Under the assumption of simple harmonic motion,

$$\eta \propto \cos(\omega t + \epsilon) \quad (8)$$

and Equation 7 becomes

$$g \frac{\partial}{\partial x} \frac{\partial \eta(x)}{\partial x} + \omega^2 \eta(x) = 0 \quad (9)$$

If we now substitute $d(x) = d_a x/a$ and $K = \omega^2 a/g d_a$ where d_a is the water depth at the gage location some distance $x = a$ from the shoreline in Equation 9 we get,

$$\frac{\partial}{\partial x} \left[x \frac{\partial \eta(x)}{\partial x} \right] + k \eta(x) = 0 \quad (10)$$

The solution to Equation 10 is

$$\eta(x) = AJ_0(2k^{1/2} x^{1/2}) \quad (11)$$

or with the time dependence restored

$$\eta(x,t) = AJ_0(2k^{1/2} x^{1/2}) \cos(\omega t + \epsilon). \quad (12)$$

Because a tsunami has a very long wave length, we can assume the entire local water surface oscillates in the vicinity of some local depth, d , where $x \geq a$, thus

$$\eta(x) = C \cos(\omega t + \epsilon) \quad (13)$$

for $x \geq a$. Equating equations 12 and 13 yields

$$A = \frac{C}{J_0(2k^{1/2} a^{1/2})} \quad (14)$$

Therefore

$$\eta(x) = C \frac{J_0(2k^{1/2} x^{1/2})}{J_0(2k^{1/2} a^{1/2})} \cos(\omega t + \epsilon) \quad (15)$$

Solving for C at $x = a$

$$C = \frac{\eta(a)}{\cos(\omega t + \epsilon)} \quad (16)$$

From Equation 15,

$$\eta(b) = C \frac{J_0(2k^{1/2} b^{1/2})}{J_0(2k^{1/2} a^{1/2})} \cos(\omega t + \epsilon) \quad (17)$$

and substituting Equation 16

$$\eta(b) = \frac{J_0(2k^{1/2} b^{1/2})}{J_0(2k^{1/2} a^{1/2})} \eta(a) \quad (18)$$

Since $\eta(a)$ is known from the numerical simulation, η at $x = b$ can be determined. The values of a , b and d_a are determined from U. S. Coast and Geodetic Survey charts.

20. Because the method described above is one dimensional, it accounts for the effects of shoaling and reflection but not refraction or diffraction. However, since a tsunami wavelength is so great in waters deeper than 600 ft, few bathymetric features are large enough to significantly refract or diffract the waves over the relatively short distance from the nearest gage location to the 600 ft contour.

VII. Results

21. Table 2 shows a comparison of amplitudes of the leading wave of the 1960 Chili tsunami as recorded by tide gages at selected exposed locations with results of the numerical simulation at locations nearest the tide gages. To avoid the false appearance of exact agreement at locations such as Port Hueneme, the results of the numerical simulation are rounded to the nearest hundredth foot rather than the nearest tenth.

Table 2
Comparison of Elevations of Maximum Rise of Initial Wave
of 1960 Peru-Chile Tsunami to Numerical Simulation

<u>Gage Location</u>	<u>1960 Peru-Chile Tsunami (feet)</u>	<u>Numerical Simulation (feet)</u>
La Jolla, Calif.	1.4	1.05
San Clemente Island, Calif.	0.9	0.89
Port Hueneme, Calif.	1.9	1.86
Presidio (San Francisco), Calif.	1.3	1.46
Crescent City, Calif.	1.3	1.02
Neah Bay, Wash.	0.9	0.73

22. Ideally, the amplitudes resulting from the simulation should be slightly less than those recorded at corresponding tide gages because of shoaling of the wave into shallower gage locations. With the exception of the Presidio gage, this is indeed the case. Two factors which could account for the anomaly at Presidio are frictional dissipation of the actual tsunami over the shallow shelf seaward of Presidio (frictional effects are neglected in the governing equations of motion), and the inadequacy of the averaged depths used in the finite difference code to represent the small detail of the shelf accurately.

23. Figure 5 shows contours of sea surface elevation of the leading tsunami waves 15 hours after generation by simulation of the 1960 Chile quake. The reason for the extensive damage caused by the 1960 Chile tsunami in the Hawaiian Islands and Japan is evident as the highest section of the wave front is directed toward these locations. The preferential radiational patterns of non-circular uplifts are well documented (Takahashi et. al., 1962; Hatori, 1963).

24. Figure 6 shows the locations of the 64 gages used to determine the leading wave amplitude as a function of distance along the Pacific coast of the United States. Figures 7-9 are plots of the amplitude of the leading wave of tsunamis generated by hypothetical uplifts located in segments 1, 8 and 12 respectively. While tsunamis generated in segments 1 and 12 generally produce similar responses along the Pacific coast, the response to the tsunami generated in segment 8 is markedly less. This

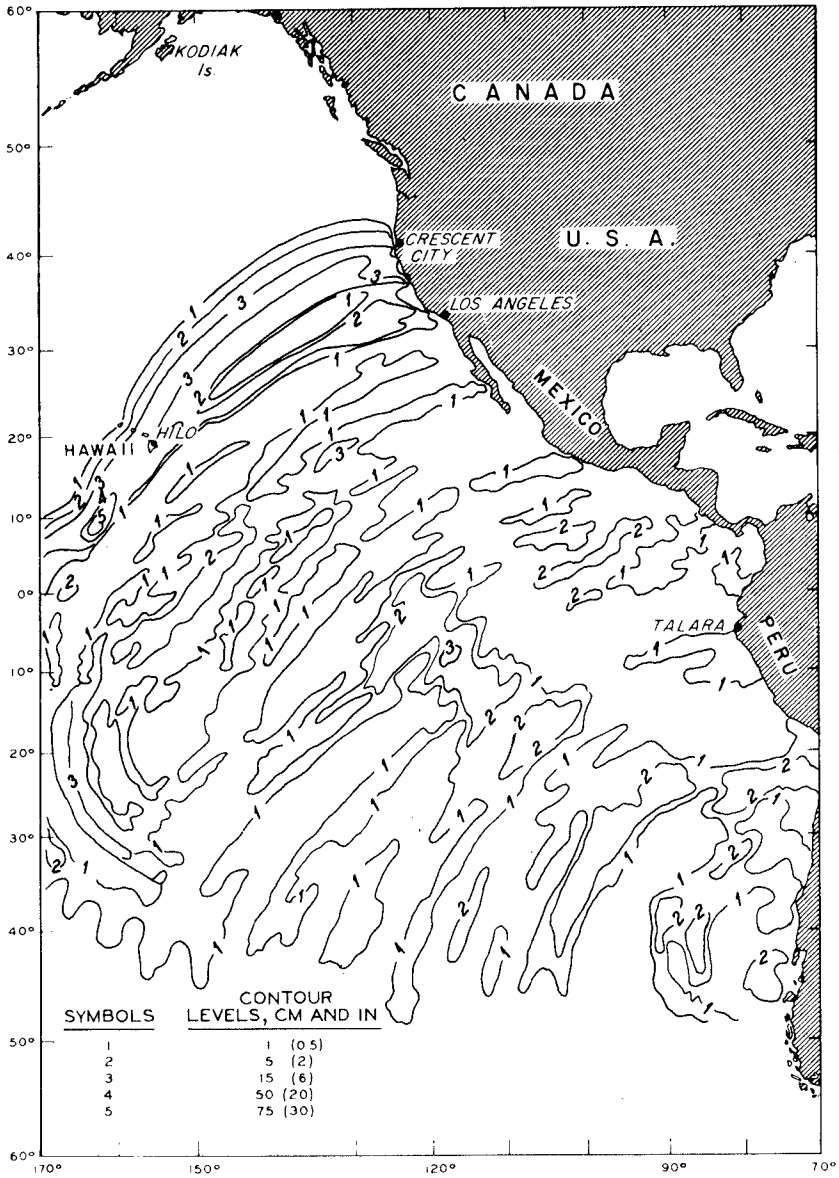


Figure 5. Contours of water-surface elevation for the leading tsunami waves 15 hrs after simulation of the 1960 Chile earthquake.

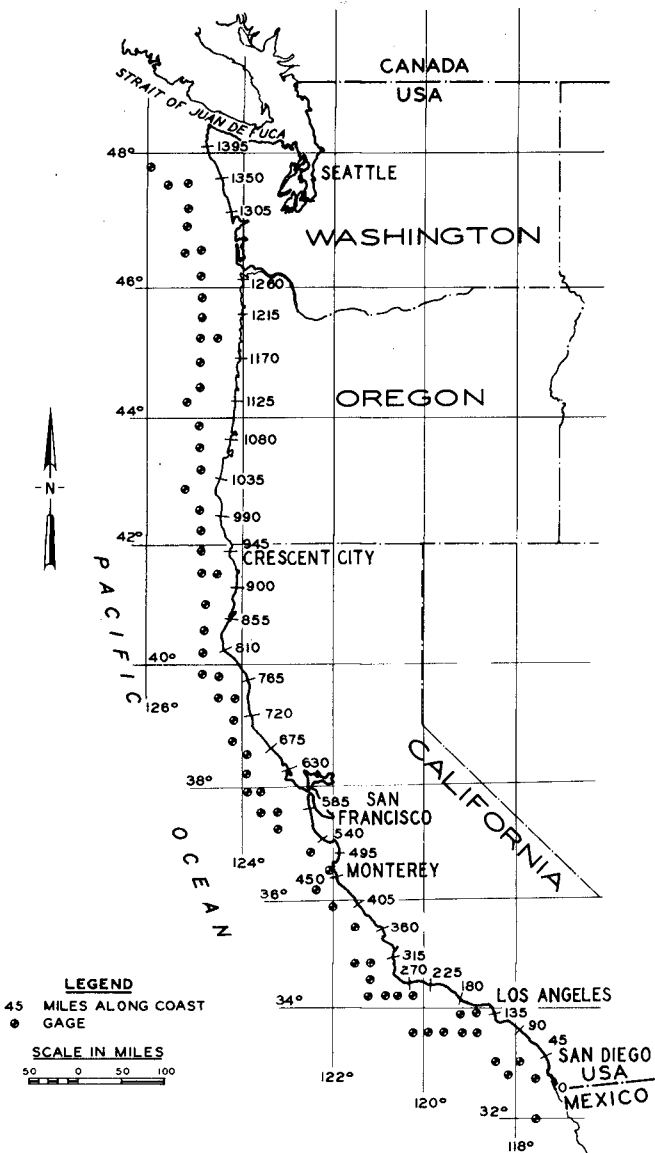


FIGURE 6. GAGE LOCATIONS ALONG THE WEST COAST

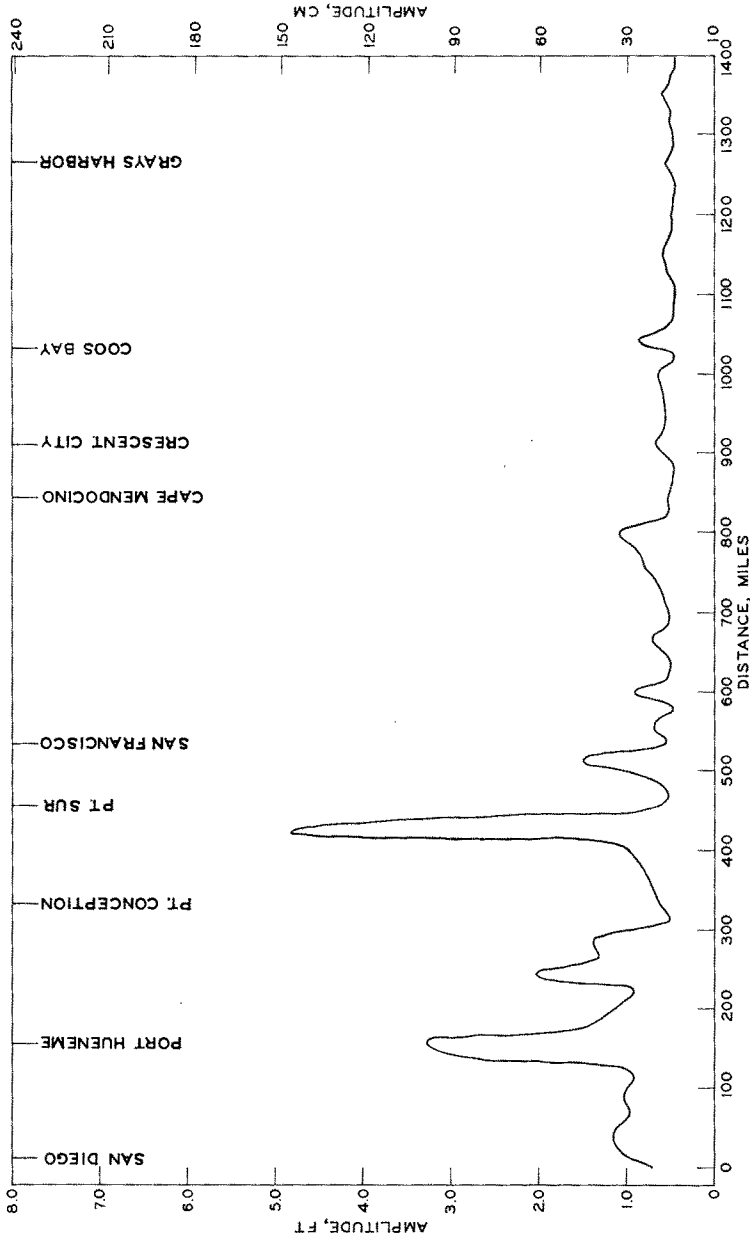


Figure 7. Wave amplitude of leading tsunami wave generated in Segment 1 versus distance of the recording gage from the U. S. - Mexico border.

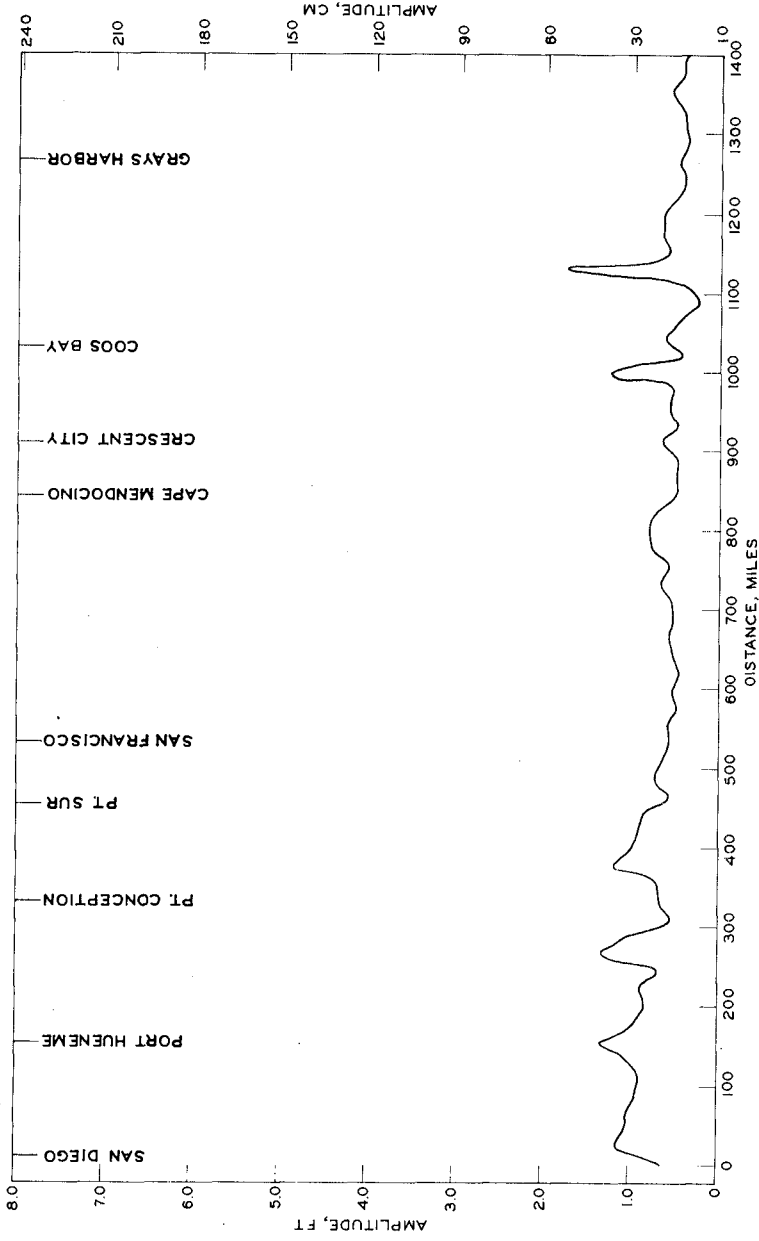


Figure 8. Wave Amplitude of leading tsunami wave generated in Segment 8 versus distance of the recording gage from the U. S. - Mexico border.

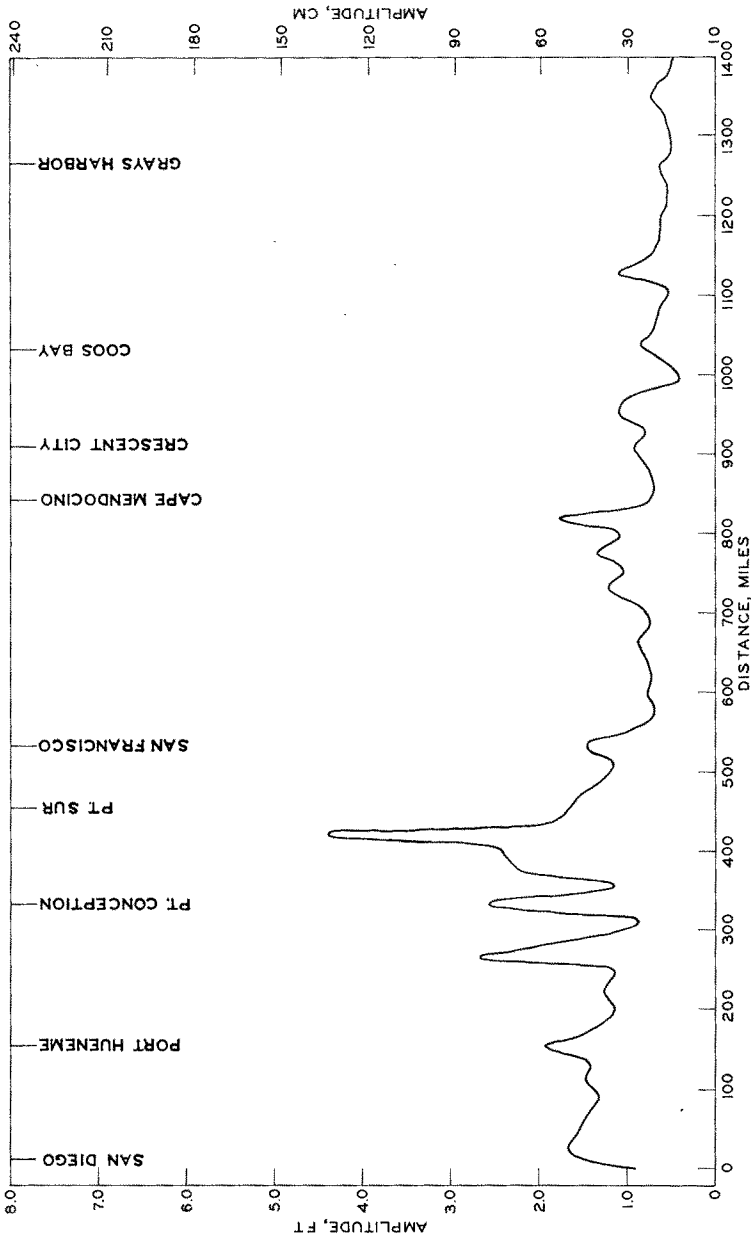


Figure 9. Wave Amplitude of leading tsunami wave generated in Segment I2 versus distance of the recording gage from the U. S. - Mexico border.

is probably due to the "shadowing" by the northwestward to southeastward oriented stretch of South American coast between 15 and 20 degrees south latitude. The generally low response exhibited along the coast from about San Diego to Los Angeles due to tsunamis generated in the three segments is probably the result of sheltering by the Channel Islands. The peaks shown in the vicinity of Port Hueneme (1.4 to 3.3 ft) agree fairly well with heights recorded there during past tsunamis, e.g., 1960 Chile, 2 ft; 1957 Aleutian, <3.5 ft. The validity of the large peaks shown in Figures 7 and 9 just south of Pt. Sur is unknown. There are no gage records existant near that location with which to compare results and it is alsb a relatively uninhabited stretch of coastline. The response of the remainder of coastline is relatively uniform with a maximum amplitude variation of about 1.5 feet. This is not unexpected due to the gradual eastward turning of the coastline as one proceeds northward.

VIII. Summary

25. The Peru-Chile Trench has a long recorded history as an area of generation of tsunamis which cause significant runup along the Pacific coast of the continental United States. An explicit numerical code has been developed and is demonstrated to adequately hindcast the Chile tsunami of 22 May 1960. The code is used to simulate the generation and propagation of tsunamis of approximately four intensity which originate in the Peru-Chile Trench. The amplitudes of the tsunamis are normalized to 600-ft depth and are plotted as a function of distance along the U. S. west coast from the Mexican to the Canadian Borders, thus allowing a relative comparison of the vulnerability of various locations along the U. S. west coast to tsunamis originating in the Peru-Chile Trench.

REFERENCES

1. Chinnery, Michael A. and North, Robert G., "The Frequency of Very Large Earthquakes," Science, Vol. 190, No. 4219, 1975.
2. Garcia, A. W. and Houston, J. R., "Type 16 Flood Insurance Study: Tsunami Predictions for Monterey and San Francisco Bays and Puget Sound," U. S. Army Waterways Experiment Station Report TR-H-75-17, 1975.
3. Hayes, D. E., "Geophysical Investigation of the Peru-Chile Trench," Marine Geology, Vol. 4, pp. 309-351, 1966.
4. Hatori, T., "Directivity of Tsunamis," Bulletin Earthquake Research Institute, Vol. 41, pp. 61-81, 1963.
5. Houston, J. R. and Garcia, A. W., "Type 16 Flood Insurance Study: Tsunami Predictions for Pacific Coastal Communities, U. S. Army Waterways Experiment Station Report TR-H-74-3, 1974.
6. Houston, J. R., Butler, H. L., Whalin, R. W. and Raney, D. C., "Probable Maximum Tsunami Runup for Distant Seismic Events - Islote Site, Puerto Rico," Amendment 23, NORCO-NP-1 PSAR, Puerto Rico Water Resources Authority, Fugro, Inc., May, 1975a.
7. Houston, J. R., Whalin, R. W., Garcia, A. W. and Butler, H. L., "Effect of Source Orientation and Location in the Aleutian Trench on Tsunami Amplitude along the Pacific Coast of the Continental United States," U. S. Army Waterways Experiment Station Report RR-H-75-4, 1975b.
8. Hwang, Li-San, Divoky, D. and Yuen, A., "Amchitka Tsunami Study," Tetra-Tech Report TC-177, 1970.
9. Kelleher, John A., "Rupture Zones of Large South American Earthquakes and some Predictions," J. Geophysical Research, Vol. 77, No. 11, pp. 2087-2103, 1972.
10. Kelleher, John, Sarvins, J., Rowlett, H., and McCann, W., "Why and Where Great Thrust Earthquakes Occur Along Island Arcs," J. Geophysical Research, Vol. 79, No. 32, pp. 4889-4899, 1974.
11. Lamb, Horace, Hydrodynamics, 6th ed., Dover Publications, New York, 1945.

12. Plafker, G., and Savage, J. C., "Mechanism of the Chilean Earthquakes of May 21 and 22, 1960, Geo. Soc. America Bull., Vol. 81, No. 4, pp. 1001-1030, 1970.
13. Smith, S. M., Menard, H. W. and Shorman, G., "World-Wide Ocean Depth and Continental Elevations Averaged for Areas Approximating One Degree Squares of Latitude and Longitude," Scripps Institution of Oceanography, La Jolla, Calif., March 1966.
14. Sykes, Lynn R., "Aftershock Zones of Great Earthquakes, Seismicity Gaps and Earthquake Prediction of Alaska and the Aleutians," J. Geophysical Research, Vol. 76, No. 32, pp. 8021-8041, 1971.
15. Symons, J. M. and Zetler, B. D., "The Tsunami of May 22, 1960 as recorded at Tide Stations," U. S. Department of Commerce, Coast and Geodetic Survey, Preliminary Report.
16. Takahashi, R. and Hatori, T., "A Model Experiment on the Tsunami Generation from a Bottom Deformation Area of Elliptic Shape," Bulletin Earthquake Research Institute, Vol. 40, pp. 873-883, 1962.

APPENDIX A: NOTATION

a	Distance along x-axis, ft
A	Amplitude constant
C	Amplitude constant
d	Depth of Water
d_a	Water depth a distance "a" from shore
e	Base of natural logarithms
g	Acceleration of gravity
J_0	$J_0()$ Zeroth order Bessel function of the first kind
k	Variable, ft^{-1}
L	Characteristics length of the wave in its direction of propagation
n	Refers to a time, $n\Delta t$
R_e	Radius of the earth
t	Time
U	Depth-averaged wave velocity component in the θ direction
V	Depth-averaged wave velocity component in the ϕ direction
x	Distance, ft
Δt	Length of a half-time step
ϵ	Phase factor
η	Wave elevation from reference water level
θ	Latitude measured from the north pole
ϕ	Longitude measured from Greenwich
ω	Wave frequency, sec^{-1}
∂	Partial differential